Earthquakes and Structures, *Vol. 14, No. 3 (2018) 249-259*
DOI: https://doi.org/10.12989/eas.2018.14.3.249

Seismic risk assessment of concrete-filled double-skin steel tube/moment-resisting frames

Yi Hu[1a], Junhai Zhao[*1], Dongfang Zhang[1] and Yufen Zhang[2]

[1]*School of Civil Engineering, Chang'an University, Xi'an 710061, China*
[2]*School of Civil Engineering, North China University of Technology, Beijing 100041, China*

(Received April 4, 2017, Revised February 7, 2018, Accepted February 14, 2018)

Abstract. This paper aims to assess the seismic risk of a plane moment-resisting frames (MRFs) consisting of concrete-filled double skin steel tube (CFDST) columns and I-section steel beams. Firstly, three typical limit performance levels of CFDST structures are determined in accordance with the cyclic tests of seven CFDST joint specimens with 1/2-scaled and the limits stipulated in FEMA 356. Then, finite element (FE) models of the test specimens are built by considering with material degradation, nonlinear behavior of beam-column connections and panel zones. The mechanical behavior of the concrete material are modeled in compression stressed condition in trip-direction based on unified strength theory, and such numerical model were verified by tests. Besides, numerical models on 3, 6 and 9-story CFDST frames are established. Furthermore, the seismic responses of these models to earthquake excitations are investigated using nonlinear time-history analyses (NTHA), and the limits capacities are determined from incremental dynamic analyses (IDA). In addition, fragility curves are developed for these models associated with 10%/50yr and 2%/50yr events as defined in SAC project for the region on Los Angeles in the Unite State. Lastly, the annual probabilities of each limits and the collapse probabilities in 50 years for these models are calculated and compared. Such results provide risk information for the CFDST-MRFs based on the probabilistic risk assessment method.

Keywords: concrete-filled double-skin steel tube; beam-column joint; unified strength theory; seismic fragility; risk assessment

1. Introduction

Concrete-filled steel tube (CFT) components are widely used in high-rise building and bridge structures for their excellent compression capacity and seismic resistance. In recent years, a new steel-concrete composite structure is know as concrete-filled double skin steel tube (CFDST) is developed based on the CFT, and it exhibits lighter weight, higher strength, better seismic and fire resistance by comparing with the CFT for the following reasons (Clark 1994, Han *et al*. 2003, Zhang and Zhang 2015). The core concrete can restrain the local buckling occurred in steel tubes, and the arrangement of inner and outer tube can significantly increases the strength and ductility of concrete. Such CFDST column has a smaller cross section by comparing with the CFT column, thus it exhibits less self-weight. For the concrete has low thermal conductivity, the inner tube could be protected by core concrete once the outer tube failed in the fire.

To investigate the mechanical property and seismic behavior of CFDST structures, a number of experimental and numerical studies had been conducted on CFDST components. It is found that the core concrete of a CFDST column worked in tri-axially confined by axial pressure generated by gravity load and lateral pressure induced by steel tubes for the different expansion rates of core concrete and steel tubes (Clark 1994, Han *et al*. 2010), and quasi-static tests had been conducted to demonstrate such point of view. 26 CFDST columns were tested under axial compression by Wei *et al*. (1995) to investigate the mechanical behavior of CFDST columns, and it was found that about 10%-30% increments on ultimate loading capacity of CFDST by comparing with the steel tubes and concrete columns alone. The effects on cross section geometry of the mechanical behavior for CFDST were studied by Han *et al*. (2006), Fan *et al*. (2008). The parameter on hollowness ratio of CFDST column were investigation through axial compression tests were performed by Uenaka *et al*. (2010). Experiment studies were conducted to analyze the failure modes of CFDST columns under different loading cases (Dong and Ho 2012, Uenaka and Kitoh 2012). Zhang *et al*. (2015) conducted blast tests and numerical studies on CFDST columns to analyze the dynamic behavior of CFDST columns.

So far, lots of researches have been conducted to understand the mechanical behavior on CFDST columns, however, very little research has been done to investigate the behavior of CFDST structures. In recent years, cyclic tests on CFDST columns-ring RC beam and CFDST columns-steel beam joints were presented and conducted (Zhang and Zhang 2015, Zhang *et al*. 2012). Such joint that connecting CFDST column and I-section steel beam was designed consists of mainly vertical stiffeners and embedded anchorage plate to cater for the seismic

∗Corresponding author, Professor
E-mail: zhaojh@chd.edu.cn, hyi_1991@163.com
[a]Ph.D.

http://www.techno-press.com/journals/eas&subpage=7
ISSN: 2092-7614 (Print), 2092-7622 (Online)

requirements of "strong column-weak beam" philosophy. At present, there is not any experimental and numerical studies have been conducted on seismic behavior of CFDST structures, including cyclic tests on CFDST plane frame and efficient numerical model on CFDST structures according to the current knowledge of the author. To ensure the seismic safety of the CFDST structure, it is important to conduct seismic mechanism analysis on whole structure (Ye and Jiang 2018).

To estimate the potential seismic damages and losses associated with CFDST structures, the seismic performance should be quantitatively measured through risk assessment on this structure. Structural reliability concepts and probabilistic risk assessment methods provide essential frameworks to manage the uncertainties associate with earthquake prediction and structural response (Cornell *et al*. 2002, Ellingwood and Kinali 2009). These methods involve not only the seismic hazard, or the potential of damaging or life-threatening earthquake, but also the structural responses and damage consequences (Li *et al*. 2010). Such a risk assessments of a building structure generally requires not only an evaluation of their dynamic responses to a spectrum of earthquakes, but also an assessment of the seismic hazard be characterized at a specific site. Taking the Los Angeles for example, which is in a high-seismic zone, the seismic hazard is described in the seismic hazard maps developed by the United State Geological Survey (USGS 2012). Seismic hazard curves were formed to quantify the ground motion at which a building would have a low probability of damage or collapse, and the shape and scale parameter were used to distinguish the seismic hazard at different sites. Furthermore, seismic fragility analyses were developed to describe the exceeding probability of a certain interesting damage limits. The building fragility curves were generated assuming a lognormal distribution, and the distribution parameters consist of the median and logarithmic standard deviation of structural capacity. The parameters is desirable obtained from experimental investigations, however, in most cases, these parameters were determined based on expert judgment. More accurate fragility parameters were acquired from the nonlinear dynamic history analyses at the present time, including incremental dynamic analysis (IDA). At present, fragility curves for steel frame structures are available from HAZUS (1997), a seismic loss estimation software proposed by the FEMA (2000). However, such method have not yet established for the CFDST structures according to the present knowledge of the author, and their performance limits have not been defined.

The current study aims to implement concrete-filled double skin tube into frame building structures and evaluate the CFDST joints performance in reducing the seismic risk of moment-frames. Firstly, six 1/2-scaled CFDST joints and a CFST joint were tested to acquire the performance levels of this lateral system, and the experimental results show the limited deformation capacity and loss of resistance of this system. Besides, verified finite element method was used to predict the nonlinear behavior of the CFDST, and a series of numerical models, including 3-story, 6-story and 9-story CFDSTs, were established to conduct nonlinear response history analyses to investigate the dynamic performance of these systems. Then, fragility curves of these systems were developed subject to different levels of earthquake inputs. Lastly, probabilities of each performance levels per year and over a period of 50 years are acquired by considering the fragilities with the seismic hazard for Los Angeles region.

2. Definition on performance limit of CFDST structures

A total of 6 CFDST joints and a square CFT joint were tested by Zhang *et al*. (2015), which were designed at a 1/2-scaled, and were approximately 2450 mm length and 1944 mm height. The detailed information of such test specimens could be found in the previous study that conducted by the Zhang *et al*. (2015), and the diagram of the constructional details of these tested joints is show in Fig. 1. The variables considered in the selection of the connections include the following:

The thickness of the outer tube; 2. The length of the extension of vertical stiffener; 3. The axial compressive force ratio; 4. With or without ribs in anchorage plate.

According to the failure modes obtained from the cyclic test for the specimens, three stages were appeared in the failure process of the test specimens in which can be divided as elastic stage, elastic-plastic stage and damage stage. At the elastic stage, the load-displacement curves were approximately linear, and no obvious phenomenons were observed in the specimens. There were also no obvious shearing deformation detected at the panel zones of the specimens (Zhang and Zhang 2015). This stage terminated when the relative story drift ratio (SDR) was about 1% for the test specimens. After that, with the development of the load, the load-displacement curve did not follow with linear relationship, and changed to the non-linear relationship. Local buckling occurred on the flange of the beam and on the local part of the outer-tubes nearby the stiffeners (Zhang and Zhang 2015). The shearing deformation of the panel zone still behaved in elastic. This stage terminated when the SDR was 2.5% in which value corresponding to the ultimately loading capacity. While in the damage stage, the strength of the specimens were

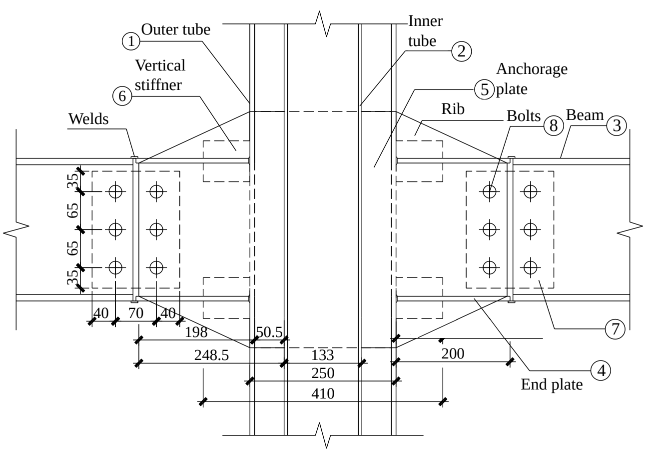

Fig. 1 Construction details of the test specimens

degrading, and cracks were appeared at the flange and web of the I-section steel beam (Zhang and Zhang 2015). With increasing the beam displacement. the cracks at the end of the steel beam and the welds nearby the high-strength bolts developed rapidly. Lastly, the specimens failed with tearing occurred in the steel beams, the SDR was about 5% at the end of this stage. Fig. 1 shows the load-displacement curves of the test specimens.

Three typical mechanical phases might be concluded: (1) Phase I: from 0 to 1% drift. The steel frame and steel tube exhibited in approximate elastic behavior; (2) Phase II: from 1% to 2.5% drift. Obviously local buckling appeared on the flange of steel beam and steel tube, fractures occurred on the steel beam nearby the high-strength bolts; (3) Phase III: from 2.5% to 5% drift. The plate on the steel beam nearby the column and high-strength bolts teared, the CFDST lost its loading capacity.

The value of the maximum of inter story drift ratio (ISDAmax) is recommended by FEMA 356 (2000), HAZUS (1997) and SEAOC (1999) to describe the performance limits of the structures. Three performance limits were classified for the building structures for the definition of FEMA 356, which had been commonly used in steel moment frames. Such performance limits were defined as Immediate Occupancy (IO), Structural Damage (SD) and Collapse Prevention (CP). However, the current version of FEMA 356 did not define the performance limits for the CFDST-MRFs, and such information have not been supplied by other specifications.

In this paper, the performance limits of the CFDST-MRF structures are determined by considering the definition of FEMA 356 for steel frame structures and the test results, and the detailed definition of the three levels are illustrated as follows:

(1) Immediate Occupancy (IO): the buildings need to be occupied immediately following the earthquake. For steel moment frames, this level can be described as: minor local yielding at a few places; no fractures; minor buckling or observable permanent distortion of members. For the CFDST structures, this level can be described as: minor yielding or buckling appeared in the flange or web of the steel beam, no obvious phenomenons observed. Thus this limit state is defined as 1.0% which is large than the value of steel moment frame by considering the test results defined in phase I of CFDST joint.

(2) Structural Damage (SD): significant damage or partial collapse of structural or nonstructural elements may occur, but the building still have some margin against total collapse, and this performance level is denoted as Life Safety in FEMA 356. For steel moment frames, it can be described as: hinges form; local buckling of some beam elements; severe joint distortion; isolated moment connection fractures, but shear connections remain intact; a few elements may experience partial fracture. For the CFDST structures, it can be described as: many plate on the steel beams nearby the column yield, buckle or fracture but do not totally fail, local buckling or hinges appeared in some elements. According to the test results defined in phase II, this limit state is estimated as 2.5%, which is similar with the steel moment frames.

Collapse Prevention (CP): the structure can not support its own gravity or it have little lateral stiffness to resist the lateral loads. For steel moment frames, this performance level can be concluded as: extensive distortion of beams and column panels; many fractures at moment connections, but shear connections remain intact. For the CFDST structures, it can be described as the steel beam tears, the concrete in the joints crush and severe buckling at the outer tube. According to the hysteretic curve presented in Fig. 2 and the test results defined in phase III, this limit state is defined as 5.0% in this paper which is similar with the steel moment frames.

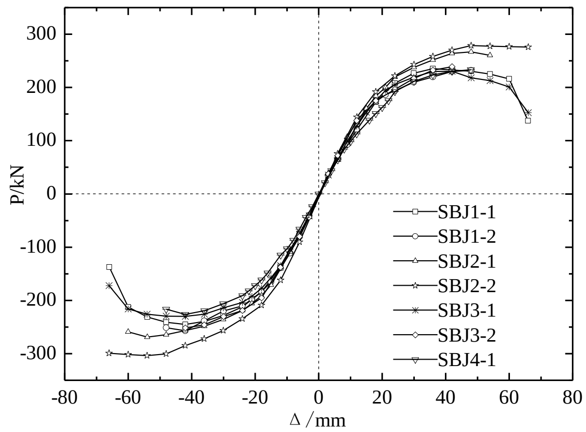

Fig. 2 Load-displacement curves of the test specimens

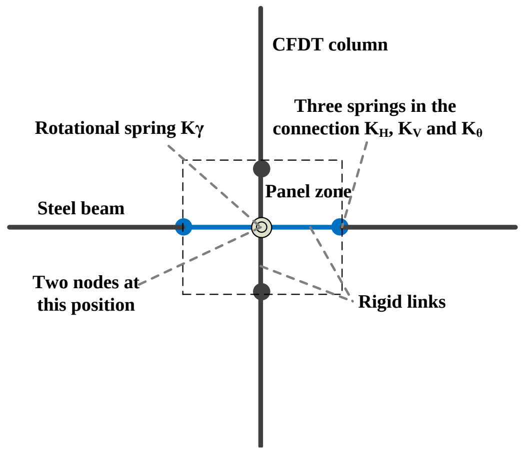

Fig. 3 Diagram of panel zone model in CFDST joints

3. Numerical model and validation

3.1 CFDST columns, steel beams and joints

The finite element software *Open System of Earthquake Engineering Simulation* OpenSees (McKenna *et al*. 2013) is used to build the numerical model of the CFDST structures, and the diagram of the numerical model is shown in Fig. 3. Nonlinear beam-column elements were used to simulate the mechanical behavior of CFDST column and steel beam. The “Concrete 02” material in OpenSees was used for the concrete core in the CFDST column, while the “Steel 02” material was used to modeling the steel tube and steel beam. As shown in Fig. 4, the Kent-Scott-Park concrete

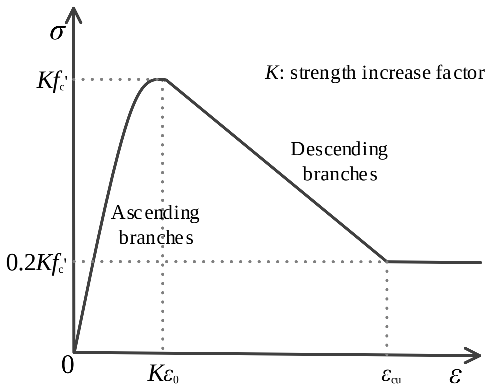

Fig. 4 Diagram of the Kent-Scott-Park concrete model

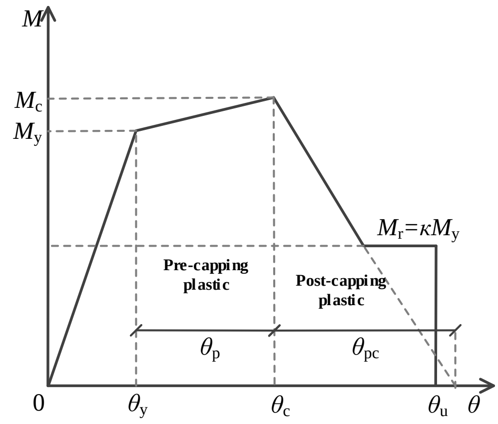

Fig. 5 Diagram of modified IK model

model (Scott *et al*. 1982) was used to simulate the hysteretic behavior of the concrete material which exhibits material deterioration.

Three springs (one horizontal K_H, one vertical K_V and one rotational K_θ) are used to model the beam-column connections, and Zero-Length element in OpenSees is chosen to simulate the mechanical behavior of the springs. In the numerical model, the horizontal one K_H is modeled with the same horizontal displacement in the two nodes on the beam and column at the connecting position. However, both the vertical one K_V and the rotational one K_θ are modeled as idealized elastic-plastic model, and the values of the elastic stiffness of K_V and K_θ and corresponding yielding strength of these springs are determined by EC3 (2005) and Skalomenos *et al*. (2015).

According to the observed failure modes of the test program, local buckling and fracture behavior occurred on the steel beam which result in deterioration in strength and stiffness of the beam-column connections. Thus simply inelasticity model may be limited to simulate the steel beam. To accurate simulate the complex behavior of steel beam, a modified energy-based phenomenological deterioration model developed by Lignos and Krawinkler (2011) is selected. Such model was developed taking basis of the Ibarra-Krawinkler (IK) model (Ibarra *et al*. 2005) and more than 300 experiments on steel WF beams. Fig. 5 shows the monotonic curve model for the modified IK model. There are three strength parameters (effective yield moment M_y, capping moment M_c, and residual moment M_r) and four deformation parameters (yield rotation θ_y, pre-capping plastic rotation θ_p, post-capping plastic rotation θ_{pc}, and ultimate rotation capacity θ_u). The detailed calculating procedures were proposed by Lignos and Krawinkler (2011). Appropriate reductions in the ultimate strength and inelastic deformation should be modified by considering the cyclic deterioration (PEER/ATC 2010). The following values should be modified: (a) the capping strength M_c is determined as 0.9 times of the initial value but no less than M_y; (b) the pre-capping plastic rotation θ_p is determined as 0.7 times of the initial value; (c) the post-capping rotation θ_{pc} is selected as 0.5 times of the initial value.

In this study, the deterioration behavior occurred in the steel beam is modeled by the rotational spring through the modified IK model for the mainly damaged behavior observed in steel beam was located near by the column according to the test results. The vertical springs are modeled as elastic-perfectly according to the recommendation of EC3 (2005). Thus the steel beams are modeled as bilinear strengthening model.

3.2 Panel zone

The panel zone (PZ) model is used to simulate the nonlinear behavior of the panel in the CFDST joint. The PZ model should considers the effects of concrete cracking, concrete crashing and steel yielding, and such effects are modeled by a certain of elements in OpenSees. The panel zone is the core region of the beam and column joints, thus the width and the height of the panel zone in this paper are 250 mm (the width of the outer tube) and 244 mm (the height of the steel beam), respectively. An inelastic-trilinear shear-deformation model was developed by Skalomenos *et al*. (2015) to model the panel zone in the CFT column connection, and such model is also used in this study to simulate the mechanical behavior of PZ in the CFDST joint. In this idealized model, the total shear strength is the sum of the strength of the steel tubes (inner and outer steel tubes) and concrete core at identical deformation. To determine the shear yield strength and post yielding stiffness of this idealized model, this study considers the previous studies on PZ behavior of square CFT column-to-WF beam bolted moment connection (2004) and interior end plate and through beam connections of steel beams to CFT columns (Sheet *et al*. 2013).

The PZ model of CFDST column connection is idealized as shown in Fig. 3 (Skalomenos *et al*. 2015, Castro *et al*. 2013), a rotational spring between the beam and the column to represent the relative rotation between them which is modeled by Zerolength element; two rigid links are used to model the rigid extension of the beam and column which is modeled by Rigidlink element. The rotation spring represents the mechanical behavior in the joint, including the rotation stiffness and the shearing capacity, thus it is important to model the stiffness and shearing capacity of the spring and then to simulate the nonlinear behavior of the joint plate (panel zone).

The horizontal shear strength of the joint combines the shearing strength supplied by steel tubes and concrete core, and the shearing capacity V_u can be calculated as the sum of

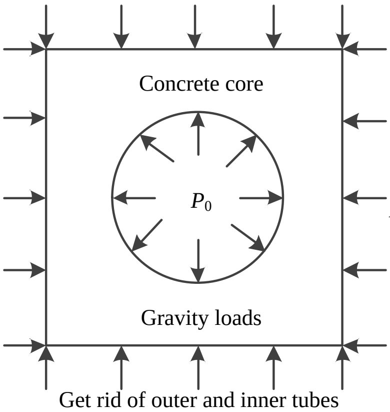

Fig. 6 Mechanical model of the core concrete in CFDST column

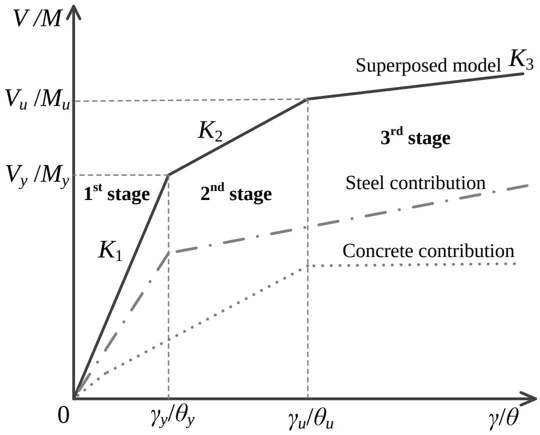

Fig. 7 Trilinear model for the panel zone in CFDST joints

the steel tubes and the concrete (Krawinkler 1978, Sheet *et al*. 2013)

$$V_u = V_s + V_c = A_{sv}(\frac{f_y}{\sqrt{3}}) + 1.99\sqrt{f_c'}A_{cv} \tag{1}$$

where A_{sv} and A_{cv} are the horizontal effective shear area of the steel tube and concrete, respectively; f_y and f_c' are the yield strength of the steel tube and the compressive strength of the concrete core, respectively.

Generally, the comprssive strength of the concrete core is larger than the nominal compressive strength of the concrete materials for the core concrete is in compression stressed condition in trip-direction caused by gravity loads. Fig. 6 shows the mechanical model of the core concrete under the gravity loads when getting rid of the outer and inner tubes. The function between the compressive strength of core concrete and the nominal strength of concrete material has been derived by Zhang *et al*. (2013) based on Unified Strength Theory which was established by Pro. Yu in 1991 at Xi'an Jiaotong University of China (2004), and it is given as

$$f_c' = f_c + k_c(P + \frac{2\zeta P_0 B}{D\sqrt{\pi}}) \tag{2}$$

$$\zeta = 66.474(\frac{t}{B})^2 + 0.992\frac{t}{B} + 0.416 \tag{3}$$

where f_c is the nominal compressive strength of concrete; k_c is the strength improvement coefficient of concrete under compressive force, and it can be determined as a constant value of 4.1 according to the test results of Zhang *et al*. (2013); ζ is the confinement reduction coefficient for the confinement of square-shape outer tube is weaken than the circular one, which can be calculated by Eq. (3); P and P_0 are the exterior and internal pressure caused by the outer and inner tube, respectively, in which there calculations have been derived by Zhang *et al*. (2013); D, B and t are the diameter of the inner tube, width of the outer tube and thickness of the outer tube, respectively.

Fig. 7 shows the idealized trilinear model for the panel zone in CFDST column-beam connections. The yielding point of the PZ is determined as the point of steel tube yielding according to the Fig. 7, and the shearing deformation can be calculated

$$\begin{aligned} \gamma_y &= \kappa_{s1} \times (\frac{V_{s1}}{A_{sv1} \times G_s}) = \kappa_{s2} \times (\frac{V_{s2}}{A_{sv2} \times G_s}) \\ V_{s1} &+ V_{s2} = V_s \end{aligned} \tag{4}$$

where κ_{s1} and κ_{s2} are the shear coefficients for a square steel tube (the outer one) and a circular steel tube (the inner one) equal to 1.2 and 10/9, respectively; A_{sv1} and A_{sv2} are the shear area of the steel outer tube and inner tube, respectively; G_s is the shearing modulus of the steel tubes. The PZ is yielding when the shearing force of it has reached 60% of the ultimate capacity V_u according to the calibration studies conducted by Muhummud *et al*. (2004) for the CFT-steel beam joints. The inelastic stiffness at 2^{nd} stage K_2 is determined as 20% of the initial stiffness at 1^{st} stage K_1.

The moment-rotation (M-θ) relationship of the rotational spring K_γ can be converted by the shear- deformation relationship presented above. The moment M and the rotation θ relationship of such rotational spring K_γ can be calculated as

$$M = V \times B, K_\theta = K_\gamma \times B, \theta = \gamma \tag{5}$$

3.3 Validation of the numerical model

Two cyclic test specimens SBJ 1-1 and SBJ 3-1 (Zhang and Zhang 2015) are selected to valid the numerical model. The outer tube and inner tube were designed as 250 mm in width and 133 mm in diameter, respectively. The thickness of the outer tube and inner tube was 8 mm and 6 mm, respectively. The I-section steel beam used for these specimens was 244×175×7×11 (height×width×web thickness×flange thickness, unit: mm). The numerical models of these specimens were built in accordance to the modeling methods presented in section 3.1 and section 3.2 of this paper.

Fig. 8 shows the comparison on the lateral load and beam displacement relationship between predicted and measured results of the test specimens. Such comparison shows that the proposed numerical modeling method by considering with the material deterioration and panel zone behavior generally agreed well with the test results. Such

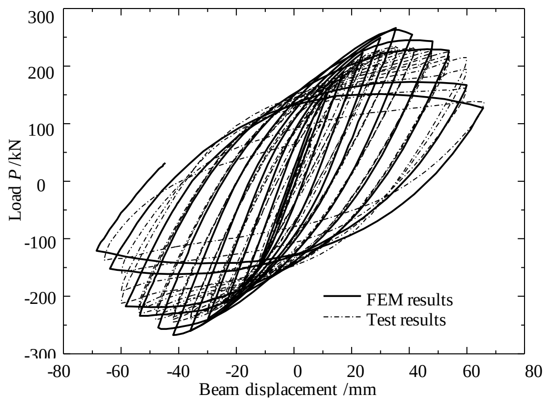

(a) SBJ 1-1

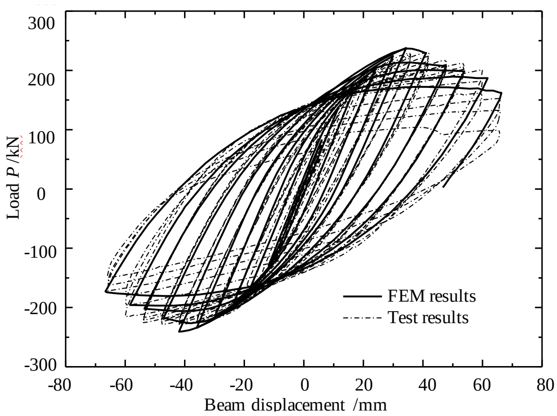

(b) SBJ 3-1

Fig. 8 Comparison of FEM and test results

numerical model also captures the cyclic stiffness and strength degradation behavior with high accuracy, thus it is demonstrates that such model is satisfactory used in predicting non-linear behavior of CFDST structures.

4. Framework for seismic risk assessment

Most risk analyses of civil infrastructure require an estimate of the probability that a structure remain in safety or serviceability limit states (Ellingwood and Kinali 2009). These limit states are related to economic loss or deaths and injuries which are cared for by stakeholders and decision-makers. Thus the risk databases of a case building are also important in seismic designation. The seismic risk assessing framework is established based on the following sources:

(1) Assembling earthquake ground motions; (2) Dynamic analyzing of the target buildings, and acquiring their responses; (3) Measuring the structural performance, and determining the damage levels; (4) Creating the fragility functions, and assessing the probability of exceedance for each performance levels; (5) Computing seismic risk and making a design decision.

The limit state probability in seismic risk assessment (Ellingwood and Kinali 2009) is given by

$$P[LS_i]=\int_0^\infty F_{\mathrm{R}}(x)F_{\mathrm{Q}}(x)\mathrm{d}x=\int_0^\infty F_{\mathrm{R}}(x)\frac{\mathrm{d}H(x)}{\mathrm{d}x}\mathrm{d}x \tag{6}$$

where Q denotes the intensity of the seismic demand which is mostly expressed as spectral acceleration in recent years; LS_i (limit state) represents the ith performance level expressed in terms of structural performance parameters such as deformations; $F_R(x)$ is cumulative distribution function of seismic capacity of a structure, and $F_Q(x)$ is the probability density function of the seismic demand; $H(x)$ is the probability that earthquake ground motion intensity exceeds x. Eq. (6) can be transformed to

$$P[LS_i]=\sum P[\mathrm{LS}_i\,|\,Q=x]P[Q=x] \tag{7}$$

where $P[Q=x]$ and $P[LS_i|Q=x]$ represent the seismic hazard and seismic fragility of a structure, respectively.

It is recommended that earthquake ground motion intensity can be represented by the Cauchy-Pareto family of distributions (Ellingwood and Kinali 2009). Thus $H(x)$ can be calculated as

$$H(x)=1-\exp[-(\frac{x}{u})^{-k}]\approx(\frac{x}{u})^{-k}=k_0x^{-k} \tag{8}$$

where k and k_0 are the shape parameter and scale parameter of the seismic hazard curves, respectively.

According to the previous seismic fragility studies of the building structures (Cornell *et al*. 2002, Ellingwood and Kinali 2009, Li *et al*. 2010), the fragility can be described by a lognormal distribution, and it is given by

$$F_{\mathrm{R}}(x)=P[\mathrm{LS}_i\,|\,Q=x]=\Phi[(\ln x-\ln m_{\mathrm{R}})\beta_{\mathrm{R}}] \tag{9}$$

where $\Phi()$ represents standard normal probability integral; m_{R} and β_R are the median capacity and logarithmic standard deviation in capacity of a structure, respectively.

Therefore, the approximate calculation of limit state probability can be calculated by substituting of Eq. (8) and Eq. (9) into Eq. (6), and the calculation is given by

$$P[\mathrm{LS}_i]\approx(k_0m_{\mathrm{R}}{}^{-k})\exp[(k\beta_{\mathrm{R}})^2/2] \tag{10}$$

5. Earthquake ground motions

Both earthquake loading and structural resistance are uncertainty for an existing building. It has been found that the uncertainty in seismic demand dominates the overall responses in comparison with the inherent variability in the capacity of the structural system (Li *et al*. 2010). Thus the parameters of the numerical models, such as yield stress and modulus, are determined as constants. In this study, a suit of 40 ground motion records are chosen to for structural risk assessment. These ground motions were developed as part of SAC project (FEMA 2010) for Los Angeles (LA) were used in the seismic risk analyses for steel buildings at this site. These records are representative of two different hazard levels: 10% (la01-20) and 2% (la21-40) probabilities of exceedance in 50 years (denoted by 2%/50yr and 10%/50yr, respectively); and each ensemble has 20 ground motions. Fig. 9 shows the response spectra from ground motions la01 through la40, represents the two hazard levels for Los Angeles.

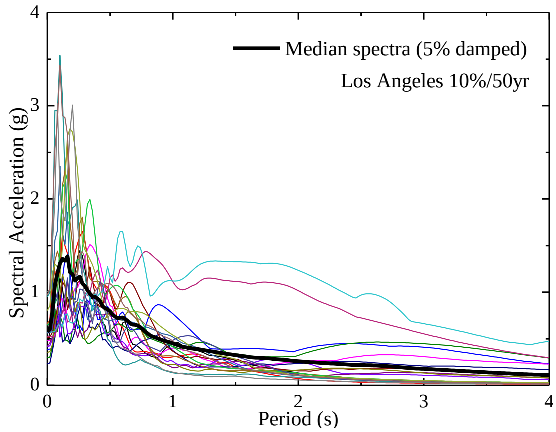

(a) la01-20

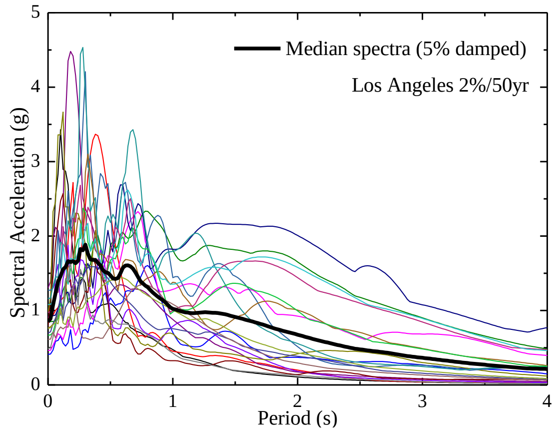

(b) la21-40

Fig. 9 Response spectra in the region of Los Angeles

Table 1 Sections and fundamental periods of CFDST-MRF models

Story	CFSTS columns	IPE beams	T_1 (s)
3	280×8 (outer tube); 133×5 (inner tube)	270 (1-3)	0.873
6	(1-4): 300×12.5 (outer tube); 160×6 (inner tube) (5-6): 300×10 (outer tube); 160×6 (inner tube)	(1-4): 330 (5-6): 300	1.421
9	(1-4): 350×12.5 (outer tube); 210×8 (inner tube) (5-7): 320×10 (outer tube); 160×6 (inner tube) (8-9): 300×8 (outer tube); 160×6 (inner tube)	(1-4): 400 (5-7): 360 (8-9): 330	1.644

6. Seismic risk assessment of CFDST-MRFs

6.1 Prototype structures

Three fixed-base planar CFT-MRFs are chosen as prototype steel structures in this study to perform the seismic fragility analysis of CFDST-MRFs. Such frames are regular design for three, six, and nine stories (the frame model with six story and the section model of CFDST column are shown in Fig. 10), and with three bays according to EC3 (2005), EC4 (2004) and EC8 (2004) presented by Skalomenos *et al.* (2015). These frames are designed with story height and bay widths equal to 3m and 5m, respectively. Such frames are selected from the study aim to present a parametric study to investigate the seismic fragility of CFDST-MRFs, and to illustrate the difference by comparing with the CFT-MRFs.

The gravity loads are assumed to G+0.3Q=27.5 kN/m (G and Q are dead and live floor loads, respectively). The yield strength of the steel material and in-filled concrete of CFDST columns are set as 275 MPa and 20 MPa, respectively. The vertical elastic stiffness of such CFDST columns are designed same with the CFT columns presented by Skalomenos *et al*. (2015). Such CFT frame was designed for vertical static load and then checked for seismic load for PGA=0.36 g, soil type B and Spectrum

Type 1 with factor q=4. The detailed information of the CFDST frames are presented in Table 1.

6.2 Probabilistic seismic demands

The seismic demands of the models are estimated based on the non-linear time history analyses (NTHA). The maximum inter-story drift angle (ISDA) is the most interest structural response in measuring damage of the models, and it expresses the potential for collapse of the structure due to the P-Δ effects. Thus ISDA is selected as the damage measure related to several performance levels in analyzed models. The inter-story drifts of each story was recorded, and the maximum ISDA is selected as the seismic demand of the model.

The relationship between maximum ISDA and first mode spectral acceleration Sa (T1) (Ellingwood and Kinali 2009) is given by

$$\theta_{\max} = a s_{a}^{b} \varepsilon \qquad (11)$$

where ε is random variable and $\sigma_{ln\varepsilon}$ denotes the uncertainty in the relationship; $\theta_{\max}$ is the maximum ISDA acquired from the NTHA; a and b are constants which are determined by the regression analysis; S_a is the spectral acceleration at the fundamental period of the structure with 5% damping ratio.

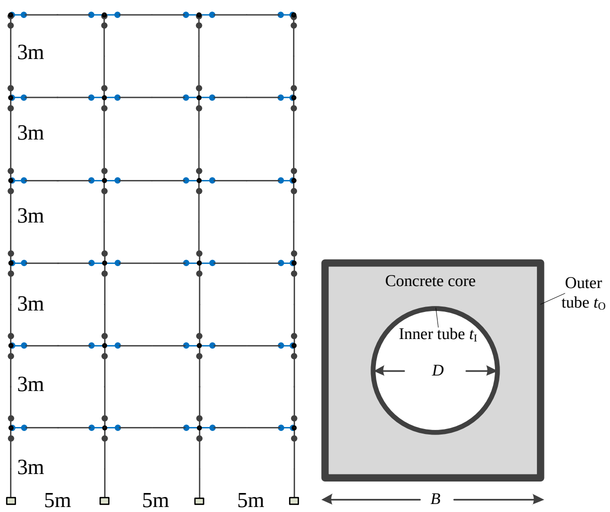

Fig. 10 Diagram of CFDST-MRF and the section of CFDST columns

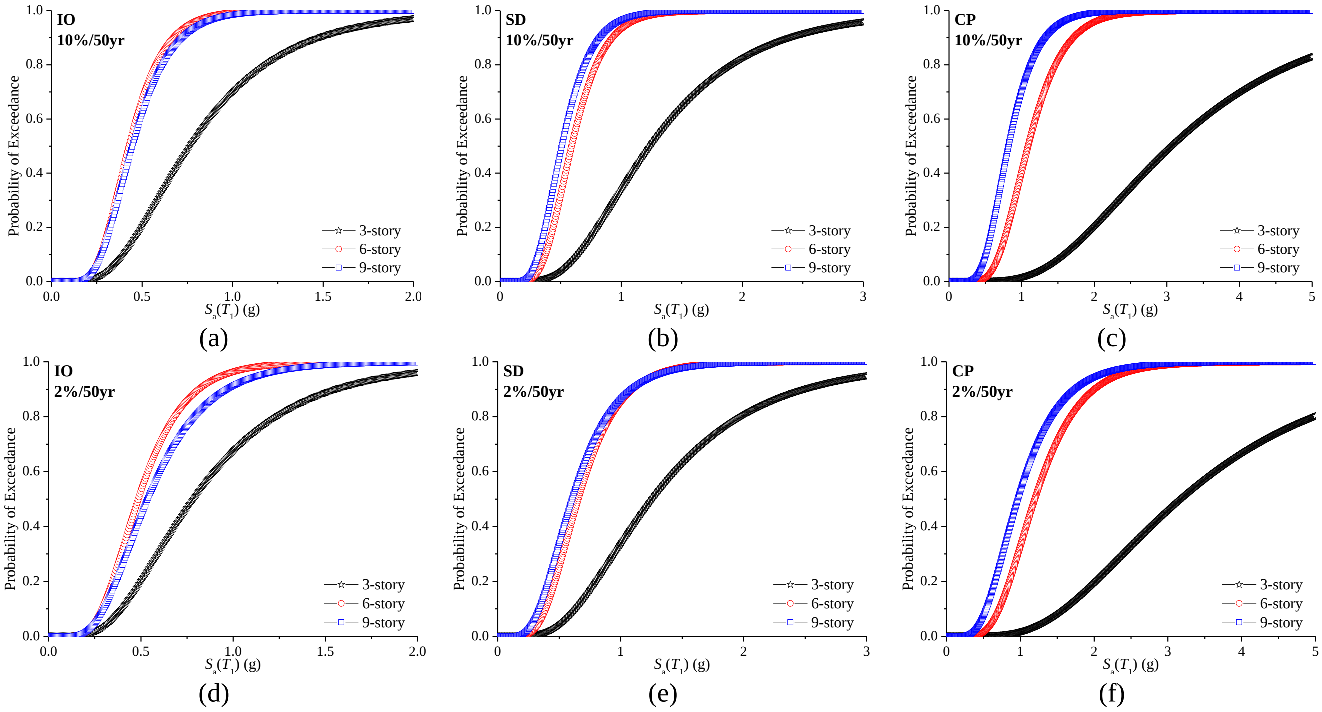

Fig. 11 Fragility curves of the models associated with LA ensemble

Table 2 Fragility parameters for the models in Los Angeles region

Models	Group	m_{IO}	m_{SD}	m_{CP}	β_R
3-story	10%/50yr	0.392	0.875	1.782	0.515
	2%/50yr	0.376	0.847	1.775	0.537
6-story	10%/50yr	0.230	0.514	1.127	0.353
	2%/50yr	0.197	0.485	1.088	0.403
9-story	10%/50yr	0.176	0.307	0.783	0.374
	2%/50yr	0.159	0.276	0.747	0.458

Note: the same value of logarithmic standard deviation is used to each limit state

6.3 Fragility curves

Incremental dynamic analyses (IDA) were performed to acquire the capacities of the models by increasing the intensity of the earthquake ground motion.

A series of nonlinear time-history analyses a structure under an ensemble of earthquake ground motion records constitute an IDA, and each record was scaled to multiple levels of various intensities (e.g., PGA) and to evaluate the seismic response of a structure in the form of inter-story drift angle (ISDA) or floor displacement. The IDA curves describe the structural responses versus earthquake intensity and determine the capacity parameters of the models. Several studies demonstrated that displacement-based response measures include $S_a(T_1)$ (g) are independent of magnitude and distance thus it is better than PGA. Therefore, the fragility function of the models can be created taking basis of the input earthquake intense in terms of $S_a(T_1)$ (g) and the exceeding probability of the interesting limit states. All the frame members are modeled by the elements used in Section 3, and the Rayleigh damping is taken as 5% in which value mass proportional only and with initial modulus.

The seismic fragility calculation was developed by substituting Eq. (11) into Eq. (8), which is given by

$$P[\mathrm{LS}_i \mid S_\mathrm{a} = x] = \Phi[\frac{(\ln ax^b / m_\mathrm{C})}{\sqrt{\beta_\mathrm{C}^2 + \beta_\mathrm{D}^2}}] \tag{12}$$

where demand variability β_D is determined by the dynamic responses of an ensemble earthquake ground motions, and the value is equal to $\sigma_{\ln\varepsilon}$; m_C is the median value for capacity which obtained from IDA. β_C is logarithmic standard deviation for capacity which is equal to $\sqrt{\beta_\mathrm{SC}^2 + \beta_\mathrm{U}^2}$, in which β_{SC} is aleatoric uncertainty in structural capacity, and β_U is epistemic uncertainty in structural modeling. In this paper, the β_C is not considered for the reason presented in Section 5 (Li *et al*. 2010).

The seismic fragilities of the CFDST-MRF models are generated by using Eq. (12), and the fragility curves associated with each limit state are shown in Fig. 11, and the corresponding fragility parameters for the fragility curves are presented in Table 2.

6.4 Probabilities estimation of annual performance limits

The seismic hazard parameters in the Los Angeles is presented in Table 3, which are obtained from USGS for both 10%/50yr and 2%/50yr earthquakes. Different parameters were acquired for the three models for the their different natural frequency (Hu *et al*. 2017). It is showed little impact on shape parameter k but large influence on scale parameter k_0. The shape parameter k are generally ranging from 1 to 4, and the value of Los Angeles is 2.69

Table 3 Seismic hazard parameters for Los Angeles region

Specimens	T_1	Hazard S_a (T_1) (g)		k	k_0 ($\times10^{-4}$)
		10%/50yr	2%/50yr		
3-story	0.873	0.845	1.268	4.067	10.611
6-story	1.421	0.519	0.779	4.065	1.462
9-story	1.644	0.449	0.673	4.079	0.803

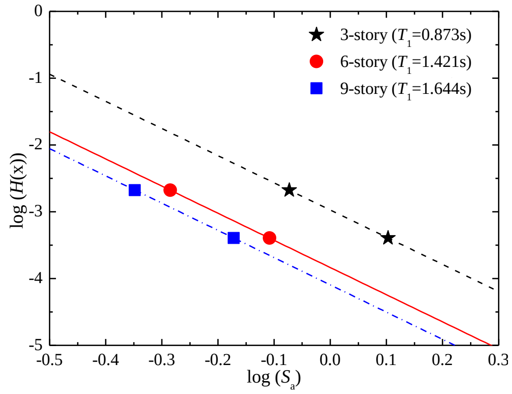

Fig. 12 Seismic hazard curves for Los Angeles

and 3.23 which calculated by Ellingwood and Kinali (2009) and Li *et al*. (2010), respectively. In this study, the shape parameter k is about 4.07 for the three models. Fig. 12 shows the seismic hazard curves generated from Table 3, which represents the probability that the spectral acceleration exceeds the determined performance limits.

The mean annual probabilities of the three models can be calculated by convolving the fragilities (presented in Fig. 11 and Table 2) in the seismic hazard curves (Table 3 and Fig. 12). The meal annual probabilities of the models are calculated by substituting the fragility parameters (Table 3) and seismic hazard parameters (Table 2) into Eq. (9), and the results are shown in Table 4.

According to the Table 4, it can be seen that the mean annual probabilities acquired from the ensemble of 2%/50yr is slightly higher than the value obtained from the ensemble of 10%/50yr. In this paper, the mean annual probabilities of the models are presented in Fig. 13(a) by selecting the results of 2%/50yr ensemble, and the Fig. 13(b) shows the relationship between collapse probability of the models in 50 years ($P_{c,50yr}$) and stories under 2%/50yr ensemble. It is found that the collapse probability of the model increases with increasing the number of stories.

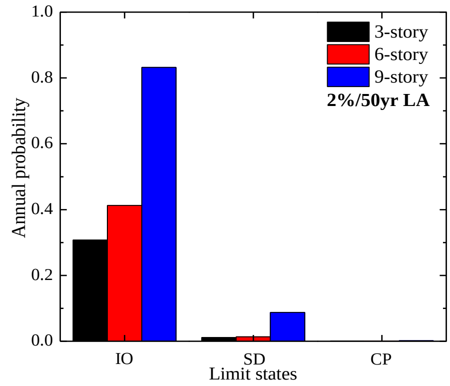

(a)

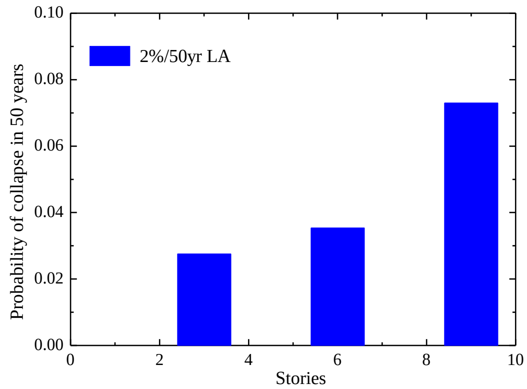

(b)

Fig. 13 (a) Annual probabilities of each limit state and (b) probability of collapse for the models in 50 years

Table 4 Annual probability of limit state occurrence for the models in Los Angeles

Specimens	Ground motion	P [LS$_i$] ($\times10^{-3}$)		
		IO	SD	CP
3-story	10%/50yr	214.51	8.19	0.46
	2%/50yr	307.74	11.32	0.56
6-story	10%/50yr	321.86	12.24	0.50
	2%/50yr	412.76	13.60	0.72
9-story	10%/50yr	614.70	63.54	1.40
	2%/50yr	831.92	87.72	1.51

7. Conclusions

Seismic risk assessments were preformed on three CFDST-MRFs with 3-story, 6-story and 9-story. Such assessments aimed at computing the probability of exceeding three performance limits during the design life time (typically is 50 years) of the structures, and the ground motions developed in the SAC project were used represent the uncertainty in earthquake demand. The following conclusions are drawn:

1. Three performance limits of CFDST structures (expressed in terms of inter-story drift angle) were determined in accordance with the failure modes of cyclic loading tests on six 1/2-scaled CFDST joints and a CFST joint and the stipulation of FEMA 356. Such limits were compared with the performance limits of steel frame structures obtained from FEMA 356.
2. Finite element model for CFDST joint was built to simulate the hysteretic behavior of tested specimen by considering material degradation, nonlinear behavior of beam-to-column joint and panel zone, such model was verified by test results. Such model considered the mechanical behavior of the concrete material subjected to compression stressed condition in trip-direction based on unified strength theory.
3. Finite element models of 3-story, 6-story and 9-story buildings were built, and ground motion records were selected from SAC project to describe the seismic hazard of Los Angeles in Unite State (divided into two

hazard levels of 2%/50yr and 10%/50yr). Such models were used to perform the nonlinear time-history analyses (NTHA) and incremental dynamic analyses (IDA) according to the selected records.

Fragility curves of the analyzing models were developed using the three determined performance limits and structural responses. The annual probabilities of these three limits and the collapse probability in 50 years were determined by convolving the fragilities with the seismic hazard specified by the USGS. The collapse probability of the model increases with increasing the number of stories.

Acknowledgments

This work was sponsored by the National Natural Science Foundation of China (51508028) and the Special Fund for Basic Scientific Research of Central College (310828173402, 310828161012, 310828173402).

References

Castro, J.M., Elghazouli, A.Y. and Izzuddin, B.A. (2013), "Modeling of the panel zone in steel and composite moment frames", *Eng. Struct.*, **27**, 129-144.

Clark, W. (1994), "Axial load capacity of circular steel tube columns filled with high strength concrete", M. Eng. Thesis, Dept. of Civil and Building Engineering, Victoria Univ. of Technology, Melbourne, Australia.

Cornell, C.A., Jalayer, F., Hamburger, R.O. and Foutch, D.A. (2002), "Probabilistic basis for 2000 SAC FEMA steel moment frame guidelines", *J. Struct. Eng.*, **128**(4), 526-533.

Dong, C.X. and Ho, J.C.M. (2012), "Uni-axial behaviour of normal strength CFDST columns with external steel rings", *Steel. Compos. Struct.*, **13**(6), 587-606.

Ellingwood, B.R. and Kinali, K. (2009), "Quantifying and communicating uncertainty in seismic risk assessment", *Struct. Saf.*, **31**, 179-187.

Eurocode 3 (2005), Design of Steel Structures, Part 1.1: General Rules and Rules for Buildings, European Standard EN 1993-1-1, European Committee for Standardization (CEN), Brussels.

Eurocode 4 (2004), Design of Composite Steel and Concrete Structures, Part 1.1: General Rules and Rules for Buildings, European Standard EN 1994-1-1, European Committee for Standardization (CEN), Brussels.

Eurocode 8 (2004), Design of Structures for Earthquake Resistance, Part 1: General Rules, Seismic Actions and Rules for Buildings, European Standard EN 1998-1-1, European Committee for Standardization (CEN), Brussels.

Fan, J., Baig, M. and Nie, J. (2008), "Test and analysis on double-skin concrete filled tubular columns", *Tubular Structures XII: Proc., Tubular Structures XII*, Taylor & Francis Group, London.

FEMA (2000), Prestandard and Commentary for the Seismic Rehabilitation of Buildings, FEMA 356, Washington, DC.

FEMA (2000), State of the Art Report on Systems Performance of Steel Moment Frames Subject to Earthquake Ground Shaking, Prepared by the SAC Joint Venture for the FEMA-355C, Washington, DC.

Han, L.H., Huang, H., Tao, Z. and Zhao, X.L. (2006), "Concrete-filled double skin steel tubular (CFDST) beam-columns subjected to cyclic bending", *Eng. Struct.*, **28**(12), 1698-1714.

Han, L.H., Yang, Y.F. and Tao, Z. (2003), "Concrete-filled thin-walled steel SHS and RHS beam-column subjected to cyclic loading", *Thin Wall. Struct.*, **41**(9), 801-833.

Han, T.H., Michael Stallings, J. and Kang, Y.J. (2010), "Nonlinear concrete model for double-skinned composite tubular columns", *Constr. Build. Mater.*, **24**(12), 2542-2553.

HAZUS (1997), *Earthquake Loss Estimation Methodology*, National Institute of Building for the FEMA, Washington, DC.

Hu, Y., Zhao, J.H. and Jiang, L.Q. (2017), "Seismic risk assessment of steel frames equipped with steel panel wall", *Struct. Des. Tall. Spec. Build.*, **26**(10), 1-12.

Ibarra, L.F., Medina, R.A. and Krawinkler, H. (2005), "Hysteretic models that incorporate strength and stiffness deterioration", *Earthq. Eng. Struct. Dyn.*, **34**(12), 1489-1511.

Krawinkler, H. (1978), "Shear in beam-column joints in seismic design of steel frames", *J. Struct. Eng.*, **15**(3), 82-91.

Li, Y., Yin, Y.J., Ellingwood, B.R. and Bulleit W.M. (2010), "Uniform hazard vs. Uniform risks bases for performance-based earthquake engineering of light-frame wood construction", *Earthq. Eng. Struct. Dyn.*, **39**(11), 1199-1217.

Lignos, D.G. and Krawinkler, H.K. (2011), "Deterioration modeling of steel components in support of collapse prediction of steel moment frames under earthquake loading", *J. Struct. Eng.*, **137**(11), 1291-1302.

McKenna, F., Fenves, G. and Scott, M. (2013), "Computer program Open-Sees: Open system for earthquake engineering simulation", Pacific Earthquake Engineering Center, Univ. of California, Berkeley, CA. (http://opensees.berkeley.edu)

Muhummud, T. (2004), "Seismic design and behavior of composite moment resisting frames constructed of CFT columns and WF beams", PhD. Thesis, Lehigh Univ., Bethlehem, PA.

PEER/ATC (2010), Modeling and Acceptance Criteria for Seismic Analysis and Design of Tall Buildings, Report No. 72-1, Applied Technology Council. Redwood City, California.

Scott, H.D., Park, R. and Priestly, M.J.N. (1982), "Stress-strain behavior of concrete confined by overlapping hoops at low and high strain rates", *J. Am. Concrete. Inst.*, **79**(1), 13-27.

SEAOC (1999), Appendix I: Tentative Guidelines for Performance-based Seismic Engineering, Part A: Strength Design Adaption, Structural Engineers Association of California, Sacramento, California.

Sheet, I.S., Gunasekaran, U. and MacRae, G.A. (2013), "Experimental investigation of CFT column to steel beam connections under cyclic loading", *J. Constr. Steel. Res.*, **86**, 167-178.

Skalomenos, K.A., Hatzigeorgiou, G.D. and Beskos, D.E. (2015), "Modeling level selection for seismic analysis of concrete-filled steel tube/moment-resisting frames by using fragility curves", *Earthq. Eng. Struct. Dyn.*, **44**, 199-220.

Uenaka, K. and Kitoh, H. (2012), "Concrete filled double skin circular tubular members subjected to pure bending and centric compressive loading", *Tub. Struct.*, XIV, 81-87.

Uenaka, K., Kitoh, H. and Sonoda, K. (2010), "Concrete filled double skin circular stub columns under compression", *Thin Wall. Struct.*, **48**(1), 19-24.

USGS (2012), U. S. Geological Survey, http://www.usgs.gov/.

Wei, S., Mau, S., Vipulanandan, C. and Mantrala, S. (1995), "Performance of new sandwich tube under axial loading: Experiment", *J. Struct. Eng.*, **121**(12), 1806-1814.

Ye, J.H. and Jiang, L.Q. (2018), "Collapse mechanism analysis of a steel moment frame based on structural vulnerability theory", *Arch. Civil Mech. Eng.*, **18**(3), 833-843.

Yu, M.H. (2004), *Unified Strength Theory and its Application*, Springer, Berlin, Heidelberg.

Zhang, F.R., Wu, C.Q., Zhao, X.L. Heidarpour, A. and Wang, H.W. (2015), "Numerical modeling of concrete-filled double-skin steel square tubular columns under blast loading", *J. Perform. Constr. Facil.*, **29**(5), B4015002-1-12.

Zhang, Y.F. and Zhang, D.F. (2015), "Experimental study on the

seismic behaviour of the connection between concrete-filled twin steel tubes column and steel beam", *Eur. J. Environ. Civil Eng.*, **19**(3), 347-365.
Zhang, Y.F., Zhao, J.H. and Cai, C.S. (2012), "Seismic behavior of ring beam joints between concrete-filled twin steel tubes columns and reinforced concrete beams", *Eng. Struct.*, **39**, 1-10.
Zhang, Y.F., Zhao, J.H. and Yuan, W.F. (2013), "Study on compressive bearing capacity of concrete-filled square steel tube column reinforced by circular steel tube inside", *J. Civil Eng. Manage.*, **19**, 787-795.

CC